

Dynamical analysis, circuit realization, and application in pseudorandom number generators of a fractional-order laser chaotic system

Chenguang Ma(马晨光), Santo Banerjee, Li Xiong(熊丽), Tianming Liu(刘天明), Xintong Han(韩昕彤), and Jun Mou(牟俊)

Citation: Chin. Phys. B, 2021, 30 (**12**): 120504. DOI: 10.1088/1674-1056/abfbd4
Journal homepage: http://cpb.iphy.ac.cn; http://iopscience.iop.org/cpb

What follows is a list of articles you may be interested in

Physical generation of random numbers using an asymmetrical Boolean network

Hai-Fang Liu(刘海芳), Yun-Cai Wang(王云才), Lu-Xiao Sang(桑鲁骁), and Jian-Guo Zhang(张建国)
Chin. Phys. B, 2021, 30 (**11**): 110503. DOI: 10.1088/1674-1056/abf4fc

A multi-directional controllable multi-scroll conservative chaos generator: Modelling, analysis, and FPGA implementation

En-Zeng Dong(董恩增), Rong-Hao Li(李荣昊), and Sheng-Zhi Du(杜升之)
Chin. Phys. B, 2021, 30 (**2**): 020505. DOI: 10.1088/1674-1056/abc239

Analysis and implementation of new fractional-order multi-scroll hidden attractors

Li Cui(崔力), Wen-Hui Luo(雒文辉), and Qing-Li Ou(欧青立)
Chin. Phys. B, 2021, 30 (**2**): 020501. DOI: 10.1088/1674-1056/abbbe4

Demodulation of acoustic telemetry binary phase shift keying signal based on high-order Duffing system

Bing-Nan Yan(燕并男), Chong-Xin Liu(刘崇新), Jun-Kang Ni(倪骏康), Liang Zhao(赵亮)
Chin. Phys. B, 2016, 25 (**10**): 100502. DOI: 10.1088/1674-1056/25/10/100502

A fractional order hyperchaotic system derived from Liu system and its circuit realization

Han Qiang, Liu Chong-Xin, Sun Lei, Zhu Da-Rui
Chin. Phys. B, 2013, 22 (**2**): 020502. DOI: 10.1088/1674-1056/22/2/020502

Dynamical analysis, circuit realization, and application in pseudorandom number generators of a fractional-order laser chaotic system*

Chenguang Ma(马晨光)[1], Santo Banerjee[3], Li Xiong(熊丽)[1,2], Tianming Liu(刘天明)[1], Xintong Han(韩昕彤)[1], and Jun Mou(牟俊)[1,2,†]

[1] School of Information Science and Engineering, Dalian Polytechnic University, Dalian 116034, China
[2] School of Physics and Electromechanical Engineering, Hexi University, Zhangye 734000, China
[3] Department of Mathematical Sciences, Giuseppe Luigi Lagrange, Politecnico di Torino, Corso Duca degli Abruzzi 24, Torino, Italy

(Received 10 February 2021; revised manuscript received 7 April 2021; accepted manuscript online 27 April 2021)

A new five-dimensional fractional-order laser chaotic system (FOLCS) is constructed by incorporating complex variables and fractional calculus into a Lorentz–Haken-type laser system. Dynamical behavior of the system, circuit realization and application in pseudorandom number generators are studied. Many types of multi-stable states are discovered in the system. Interestingly, there are two types of state transition phenomena in the system, one is the chaotic state degenerates to a periodical state, and the other is the intermittent chaotic oscillation. In addition, the complexity of the system when two parameters change simultaneously is measured by the spectral entropy algorithm. Moreover, a digital circuit is design and the chaotic oscillation behaviors of the system are verified on this circuit. Finally, a pseudo-random sequence generator is designed using the FOLCS, and the statistical characteristics of the generated pseudo-random sequence are tested with the NIST-800-22. This study enriches the research on the dynamics and applications of FOLCS.

Keywords: fractional-order laser chaotic system, SE complexity, intermittent chaos, NIST test, circuit realization

PACS: 05.45.–a, 05.45.Pq, 05.45.Gg, 05.45.Jn **DOI:** 10.1088/1674-1056/abfbd4

1. Introduction

Advantages of chaotic systems such as the extreme sensitivity to initial values, the inherent randomness, ergodicity make them prime candidates for scrambling and diffusion in image encryption process.[1–12] However, with development of technologies such as deep learning and artificial intelligence algorithms, predicting low-dimensional simple chaotic sequences has become a piece of cake.[13,14] This situation will lead some secret communication schemes based on this chaotic sequence fragile and easy to crack. Therefore, constructions of chaotic systems with high dimensionality and complex dynamical behaviors are favored by scholars.[15–19]

Laser chaotic systems are widely used in the field of optical secure communication because they can quickly generate high-dimensional broadband, high-frequency, and strong nonlinear chaotic signals.[20–28] A surging number of scholars spare no effort to study laser chaotic systems. For instance, Kadhim *et al.*[29] constructed a new four-dimensional laser chaotic system by introducing complex variables into a Lorentz–Haken system, and designed a random sequence generator based on this system, Ran *et al.*[30] constructed a new master-slave laser chaotic system, analyzed its dynamical characteristics, and used this system to construct a random sequence generator. Reports on low-dimensional laser chaotic systems are not uncommon. However, there are few reports on the construction and realization of high-dimensional laser chaotic systems.

Fractional calculus is not a novel concept, its unique memory effect makes it more suitable for describing the process-related physical phenomena, but its development has stagnated due to computational difficulties. Fortunately, fractional calculus has been applied to various fields due to the increase in computing power, such as signal processing, image detection, control systems, and financial systems.[31–35] Integer calculus, as a special case of fractional calculus, hides many properties of physical phenomena. A growing number of academicians devoted themselves to discovering special properties of fractional-order systems.[36–38] By introducing fractional calculus to a chaotic system, the bifurcation parameters of the system can be expanded, and some complex behaviors such as state transitions and bursting oscillations will appear. Therefore, fractional-order chaotic systems (FOCSs) have attracted attention of scholars.[39–48] He *et al.*[49] found through numerical simulation that time-varying order will change dynamical behaviors of an FOCS. Ma *et al.*[50] analyzed multi-stable behaviors of an incommensurate FOCS, and also analyzed the influence of order of different sub-equations in the system equation on the bifurcation be-

*Project supported by the National Natural Science Foundation of China (Grant No. 62061014) and the Natural Science Foundation of Liaoning Province, China (Grant No. 2020-MS-274).

†Corresponding author. E-mail: moujun@csu.edu.cn

© 2021 Chinese Physical Society and IOP Publishing Ltd

havior of the system. Wang *et al.*[51] analyzed the complex dynamical behaviors of an FOCS with coexisting hidden attractors and designed a circuit to verify the characteristic of the FOCS. Research and implementation of FOCSs are still in infancy, requiring further investigations by scholars.

Based on the above discussion, strong curiosity drives us to explore dynamical characteristics of a high-dimensional fractional-order laser chaotic system (FOLCS). Therefore, we propose a new five-dimensional (5D) FOLCS, analyze the dynamical behaviors, realize it by a circuit and apply it to a pseudorandom number generator (PRNG). The rest of the paper is arranged as follows: The model of the FOLCS, its properties and numerical solution process are given in Section 2. Section 3 analyzes some dynamical behaviors of the FOLCS, including some special behaviors such as state transitions and coexistence of attractors. The circuit implementation of the system and its application in the PRNG are introduced in Sections 5 and 6, respectively. Finally, some conclusions are summarized in Section 7.

2. Model of the new laser system and the numerical solution of its fractional-order form

2.1. The model and its properties of the laser chaotic system

A new Lorentz–Haken-type laser system with the host-nonlinearity is expressed as

$$\begin{aligned}\frac{\mathrm{d}x_1}{\mathrm{d}t} &= -a(x_1-x_2)+\mathrm{i}kx_1|x_1|^2,\\ \frac{\mathrm{d}x_2}{\mathrm{d}t} &= -(1-\mathrm{i}c)x_2+(f-x_3)x_1,\\ \frac{\mathrm{d}x_3}{\mathrm{d}t} &= -bx_3+\mathrm{Re}(x_1x_2).\end{aligned} \tag{1}$$

From the perspective of optical theory, $a=\frac{T_\mathrm{P}}{T_\mathrm{E}}$, $b=\frac{T_\mathrm{P}}{T_\mathrm{N}}$, and T_P donates the induced polarization, T_E means the optical field, T_N represents the inversion parameter. The state variable x_1 is proportional to the electrical field, x_2 is the induced polarization, and $f-x_3$ means the inversion. In addition, the coupling relationship between the amplitude and phase change is determined by parameter c, and the linewidth enhancement factor is represented by k. Since x_1 and x_2 can take values in the complex number domain, under the transformation $x_1=x+\mathrm{i}y$; $x_2=z+\mathrm{i}w$, $x_3=u$; $k=d+\mathrm{i}e$, the new 5D laser system can be expressed as

$$\begin{aligned}\dot{x} &= -a(x-z)-(x^2+y^2)(ex+dy),\\ \dot{y} &= -a(y-w)+(x^2+y^2)(dx-ey),\\ \dot{z} &= -(z+cw)+(f-u)x,\\ \dot{w} &= -(w-cz)+(f-u)y,\\ \dot{u} &= -bu+(xz-yw),\end{aligned} \tag{2}$$

where (x, y, z, w, $u|$ x, y, z, w, $u\in R$) are state variables, and a, b, c, d, e, f are bifurcation parameters. Obviously, the system remains unchanged under coordinate transformation (x, y, z, w, u)→($-x$, $-y$, $-z$, $-w$, u), that is, the system remains unchanged when rotated 180° around the u axis. The factors that affect the divergence of the system (2) read

$$\begin{aligned}\nabla V &= \frac{\partial\dot{x}}{\partial x}+\frac{\partial\dot{y}}{\partial y}+\frac{\partial\dot{z}}{\partial z}+\frac{\partial\dot{w}}{\partial w}+\frac{\partial\dot{u}}{\partial u}\\ &= 2y(dx-ey)-2x(dy+ex)\\ &\quad -2e(x^2+y^2)-2-b-2a.\end{aligned} \tag{3}$$

It can be seen from Eq. (3) that the divergence of the laser system is not only related to parameters, but also affected by state variables. Introducing the Caputo differential definition in the laser chaotic system (2), the 5-D FOLCS can be expressed as

$$\begin{aligned}D^q_{t_0}x &= -a(x-z)-(x^2+y^2)(ex+dy),\\ D^q_{t_0}y &= -a(y-w)+(x^2+y^2)(dx-ey),\\ D^q_{t_0}z &= -(z+cw)+(f-u)x,\\ D^q_{t_0}w &= -(w-cz)+(f-u)y,\\ D^q_{t_0}u &= -bu+(xz-yw),\end{aligned} \tag{4}$$

where q is a non-integer derivative.

In order to explore stability of the equilibrium point of the FOCS, we investigate the stability of the equilibrium points of the real number field of the system (2). Let the left side of Eq. (2) be 0, the equilibrium point can be obtained as $E_0=(0,0,0,0,0)$, and substituting E_0 into the Jacobian matrix of system (2), one can reach

$$J_{E_0}=\begin{bmatrix}-a & 0 & a & 0 & 0\\ 0 & -a & 0 & a & 0\\ f & 0 & -1 & -c & 0\\ 0 & f & c & -1 & 0\\ 0 & 0 & 0 & 0 & -b\end{bmatrix}, \tag{5}$$

and the characteristic polynomial of the matrix J_{E_0} is

$$\begin{aligned}&(\lambda+b)[\lambda^4+P_3\lambda^3+P_2\lambda^2+P_1\lambda+P_0]=0,\\ &P_3=2a+2,\\ &P_2=a^2-2af+4a+c^2+1,\\ &P_1=a(2a-2af+c^2-2f+2),\\ &P_0=a^2(c^2+f^2-2f+1).\end{aligned} \tag{6}$$

According to the Routh–Hurwitz criterion, if the following conditions are met, the equilibrium point E_0 is stable:

$$\begin{aligned}&P_i>0,\quad i=0,1,2,3,\\ &P_2P_3-P_1>0,\\ &P_1P_2P_3-{P_1}^2-P_0P_3^2>0.\end{aligned} \tag{7}$$

For simplicity, let $a=8$, $b=1$, $c=-0.36$, $d=-0.01$, $e=0.005$, $f=38$, the characteristic values at the equilibrium point E_0 are $13.2825\pm0.2154\mathrm{i}$; $-22.2825\pm0.1446\mathrm{i}$;

-1. Obviously, E_0 is an unstable saddle point under these conditions. For the FOCS, its equilibrium point will be stable if the eigenvalue of the Jacobian matrix J at the equilibrium point satisfies the following equation:

$$|\arg(eig(J))| > \frac{q\pi}{2}. \tag{8}$$

Therefore, E_0 is stable when

$$q < 2|a\tan(0.1446/22.2825)|/\pi = 0.0041.$$

2.2. The numerical solution of the FOLCS

Based on the ADM algorithm, the numerical solution of the FOLCS can be expressed as

$$\begin{aligned}\tilde{x}_j &= c_j^0 + c_j^1\frac{h^q}{\Gamma(q+1)} + c_j^2\frac{h^{2q}}{\Gamma(2q+1)}\\ &\quad + c_j^3\frac{h^{3q}}{\Gamma(3q+1)} + c_j^4\frac{h^{4q}}{\Gamma(4q+1)} + \cdots,\end{aligned} \tag{9}$$

where $j = 1,2,3,4,5$, and the step size $h = 0.01$ is always maintained in this study. In this paper, the first 5 items are intercepted, which can not only guarantee the calculation accuracy but also reduce the calculation time. Assuming the initial value $x_0 = [x_1^0, x_2^0, x_3^0, x_4^0, x_5^0]$, and the related gamma functions are represented by Eq. (10), then the coefficients c_j^i are shown as follows:

$$\begin{aligned}\Gamma 211 &= \frac{\Gamma(2q+1)}{\Gamma^2(q+1)},\\ \Gamma 311 &= \frac{\Gamma(3q+1)}{\Gamma^2(q+1)},\\ \Gamma 312 &= \frac{\Gamma(3q+1)}{\Gamma(q+1)\Gamma(2q+1)},\\ \Gamma 3111 &= \frac{\Gamma(3q+1)}{\Gamma^3(q+1)};\end{aligned} \tag{10}$$

$$c_1^0 = x_1^0,\quad c_2^0 = x_2^0,\quad c_3^0 = x_3^0,\quad c_4^0 = x_4^0,\quad c_5^0 = x_5^0; \tag{11}$$

$$\begin{aligned}c_1^1 &= -a(c_1^0 - c_3^0) - (e((c_1^0)^3 + (c_2^0)^2 c_1^0) + d((c_1^0)^2 c_2^0 + (c_2^0)^3)),\\ c_2^1 &= -a(c_2^0 - c_4^0) + (d((c_1^0)^3 + (c_2^0)^2 c_1^0) - e((c_1^0)^2 c_2^0 + (c_2^0)^3)),\\ c_3^1 &= -(c_3^0 + cc_4^0) + fc_1^0 - c_1^0 c_5^0,\quad c_4^1 = -(c_4^0 - cc_3^0) + fc_2^0 - c_2^0 c_5^0,\quad c_5^1 = -bc_5^0 + (c_1^0 c_3^0 - c_2^0 c_4^0);\end{aligned} \tag{12}$$

$$\begin{aligned}c_1^2 &= -a(c_1^1 - c_3^1) - (e(3c_1^1(c_1^0)^2 + c_1^1(c_2^0)^2 + 2c_1^0 c_2^0 c_2^1) + d(3c_2^1(c_2^0)^2 + c_2^1(c_1^0)^2 + 2c_2^0 c_1^0 c_1^1)),\\ c_2^2 &= -a(c_2^1 - c_4^1) + (d(3c_1^1(c_1^0)^2 + c_1^1(c_2^0)^2 + 2c_1^0 c_2^0 c_2^1) - e(3c_2^1(c_2^0)^2 + c_2^1(c_1^0)^2 + 2c_2^0 c_1^0 c_1^1)),\\ c_3^2 &= -(c_3^1 + cc_4^1) + fc_1^1 - (c_1^1 c_5^0 + c_1^0 c_5^1),\quad c_4^2 = -(c_4^1 - cc_3^1) + fc_2^1 - (c_2^1 c_5^0 + c_2^0 c_5^1),\\ c_5^2 &= -bc_5^1 + (c_1^0 c_3^1 + c_1^1 c_3^0 - c_2^0 c_4^1 - c_2^1 c_4^0);\end{aligned} \tag{13}$$

$$\begin{aligned}c_1^3 &= -a(c_1^2 - c_3^2) - (e(3c_1^2(c_1^0)^2 + 3c_1^0(c_1^1)^2\Gamma 211 + (c_1^2(c_2^0)^2 + 2c_1^1 c_2^0 c_2^1\frac{\Gamma(2q+1)}{\Gamma^2(q+1)} + 2c_1^0 c_2^0 c_2^2 + c_1^0 c_2^1 c_2^1\Gamma 211)),\\ &\quad + d(3c_2^2(c_2^0)^2 + 3c_2^0(c_2^1)^2\Gamma 211 + (c_2^2(c_1^0)^2 + 2c_2^1 c_1^0 c_1^1\Gamma 211 + 2c_2^0 c_1^0 c_1^2 + c_2^0 c_1^1 c_1^1\Gamma 211))),\\ c_2^3 &= -a(c_2^2 - c_4^2) + (d(3c_1^2(c_1^0)^2 + 3c_1^0(c_1^1)^2\Gamma 211 + (c_1^2(c_2^0)^2 + 2c_1^1 c_2^0 c_2^1\Gamma 211 + 2c_1^0 c_2^0 c_2^2 + c_1^0 c_2^1 c_2^1\Gamma 211)),\\ &\quad - e(3c_2^2(c_2^0)^2 + 3c_2^0(c_2^1)^2\Gamma 211 + (c_2^2(c_1^0)^2 + 2c_2^1 c_1^0 c_1^1\Gamma 211 + 2c_2^0 c_1^0 c_1^2 + c_2^0 c_1^1 c_1^1\Gamma 211)))\\ c_3^3 &= -(c_3^2 + cc_4^2) + fc_1^2 - (c_1^2 c_5^0 + c_1^1 c_5^1\Gamma 211 + c_1^0 c_5^2),\quad c_4^3 = -(c_4^2 - cc_3^2) + fc_2^2 - (c_2^2 c_5^0 + c_2^1 c_5^1\Gamma 211 + c_2^0 c_5^2),\\ c_5^3 &= -bc_5^2 + (c_1^2 c_3^0 + c_1^1 c_3^1\Gamma 211 + c_1^0 c_3^2 - c_2^2 c_4^0 - c_2^1 c_4^1\Gamma 211 - c_2^0 c_4^2);\end{aligned} \tag{14}$$

$$\begin{aligned}c_1^4 &= -a(c_1^3 - c_3^3) - (e((c_1^1)^3\Gamma 311 + (6c_1^0 c_1^1 c_1^2 + 2c_1^2 c_2^0 c_2^1 + 2c_1^1 c_2^2 c_2^0 + 2c_1^0 c_2^2 c_2^1)\Gamma 312,\\ &\quad + 3(c_1^0)^2 c_1^3 + c_1^3(c_2^0)^2 + c_1^1 c_2^1 c_2^1\Gamma 3111 + 2c_1^0 c_2^3 c_2^0) + d((c_2^1)^3\Gamma 311 + (6c_2^0 c_1^1 c_2^2 + 2c_2^2 c_1^0 c_1^1,\\ &\quad + 2c_2^1 c_1^2 c_1^0 + 2c_2^0 c_1^2 c_1^1)\Gamma 312 + 3(c_2^0)^2 c_2^3 + c_2^3(c_1^0)^2 + c_2^1 c_1^1 c_1^1\Gamma 3111 + 2c_2^0 c_1^3 c_1^0))\\ c_2^4 &= -a(c_2^3 - c_4^3) + (d((c_1^1)^3\Gamma 311 + (6c_1^0 c_1^1 c_1^2 + 2c_1^2 c_2^0 c_2^1 + 2c_1^1 c_2^2 c_2^0 + 2c_1^0 c_2^2 c_2^1)\Gamma 312,\\ &\quad + 3(c_1^0)^2 c_1^3 + c_1^3(c_2^0)^2 + c_1^1 c_2^1 c_2^1\Gamma 3111 + 2c_1^0 c_2^3 c_2^0) - e((c_2^1)^3\Gamma 311 + (6c_2^0 c_1^1 c_2^2 + 2c_2^2 c_1^0 c_1^1,\\ &\quad + 2c_2^1 c_1^2 c_1^0 + 2c_2^0 c_1^2 c_1^1)\Gamma 312 + 3(c_2^0)^2 c_2^3 + c_2^3(c_1^0)^2 + c_2^1 c_1^1 c_1^1\Gamma 3111 + 2c_2^0 c_1^3 c_1^0)),\\ c_3^4 &= -(c_3^3 + cc_4^3) + fc_1^3 - (c_5^3 c_1^0 + (c_5^2 c_1^1 + c_5^1 c_1^2)\Gamma 312 + c_5^0 c_1^3),\\ c_4^3 &= -(c_4^3 - cc_3^3) + fc_2^3 - (c_5^3 c_2^0 + (c_5^2 c_2^1 + c_5^1 c_2^2)\Gamma 312 + c_5^0 c_2^3),\\ c_5^3 &= -bc_5^3 + (c_3^3 c_1^0 + (c_3^2 c_1^1 + c_3^1 c_1^2 - c_4^2 c_2^1 - c_4^1 c_2^2)\Gamma 312 + c_3^0 c_1^3 - c_4^3 c_2^0 - c_4^0 c_2^3).\end{aligned} \tag{15}$$

When $a = 8$, $b = 1$, $c = -3.8$, $d = -0.3275$, $e = 0.003$, $f = 38$, $q = 0.9$, the initial value $x_0 = [-3, 1, 5, 10, -7]$, the attractor projections of the system are shown in Fig. 1. Under these conditions, the Lyapunov exponent (LE) of the system are 0.9058, 0, -7.9739, -34.8478, -38.2401, and the Lyapunov dimension $D_L = 2.1136$.

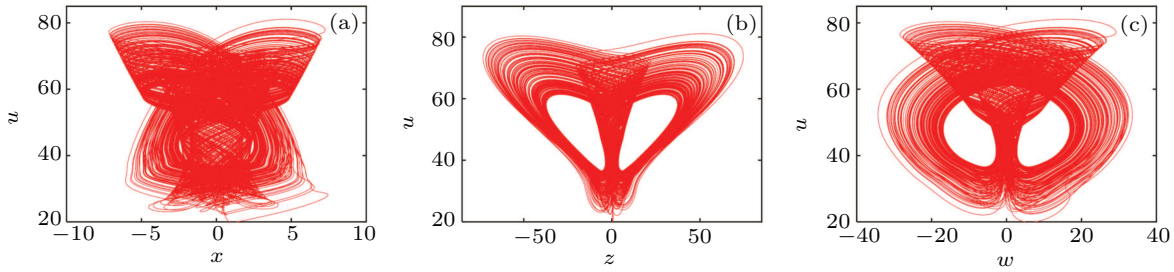


Fig. 1. The projections of attractor on (a) x–u plane, (b) z–u plane, and (c) w–u plane.

3. The dynamical behaviors of the FOLCS

3.1. Dynamical characteristics influenced by parameters and orders

It is a very effective method to explore the dynamical behaviors of the system at different orders through the bifurcation diagram and the Lyapunov exponent spectrum. Figure 2 shows the detailed bifurcation behaviors and Lyapunov exponent (LE) values of the system with the order q when $a = 8$, $b = 1$, $c = 2.1$, $d = 0.01$, $e = 0.02$, $f = 38$, with the initial value $x_0 = [1, 1, 1, 1, 1]$. The first three LEs' curves are provided here to clearly capture the changes in the system state. The data shows that when $q = 0.652$, the maximum LE (MLE) of the system is 4.018. It can be seen from Fig. 2 that the larger the orders, the smaller the LE values, which means that the randomness of the sequence generated by the integer-order system is worse than that of the fractional order.

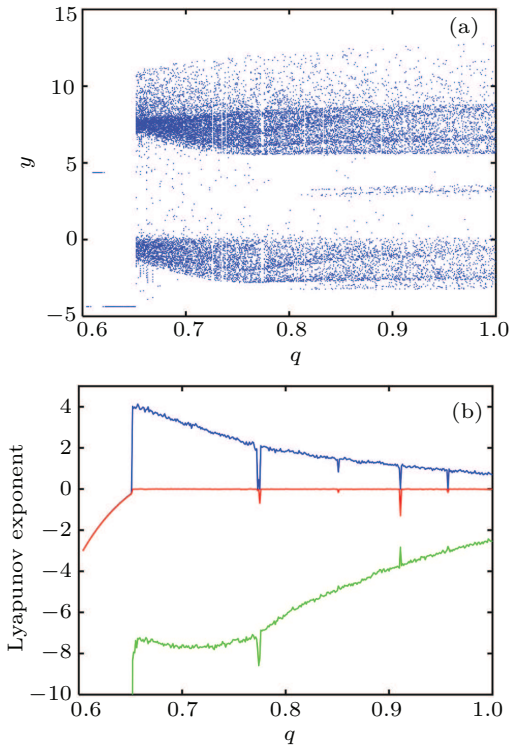


Fig. 2. Dynamical behaviors versus q: (a) bifurcation diagram, (b) Lyapunov exponent.

A conspicuous advantage of this FOLCS is that it has multiple bifurcation parameters and there are multiple paths to chaos. Taking the variable parameter c as a case, when $a = 8$, $b = 1$, $d = 0.01$, $e = 0.02$, $f = 38$, $q = 0.9$ and under the initial condition $x_0 = [1, 1, 1, 1, 1]$, the bifurcation diagram and LEs varying with parameter c are shown in Fig. 3. It can be seen from Fig. 3(a) that as the parameter c increases, the system enters a chaotic state from period-doubling bifurcation. Interestingly, the period-doubling bifurcation, boundary crises points and reverse period-doubling bifurcation can be seen clearly in the partially enlarged diagram in Fig. 4, and the data record that $c = -3.901, 3.797$ are the boundary crises points. The MLE $= 2.151$ is located at $c = 3.96$. The results of the MLE and SE complexity of the system varying with the parameter c with different orders are shown in Figs. 5(a) and 5(b). Overall, the smaller the order, the larger the MLE and the higher the SE complexity of the system. However, as the order decreases, more periodic windows appear in the system. When $q = 0.9$, the system has not only a larger chaotic range, but also a larger MLE.

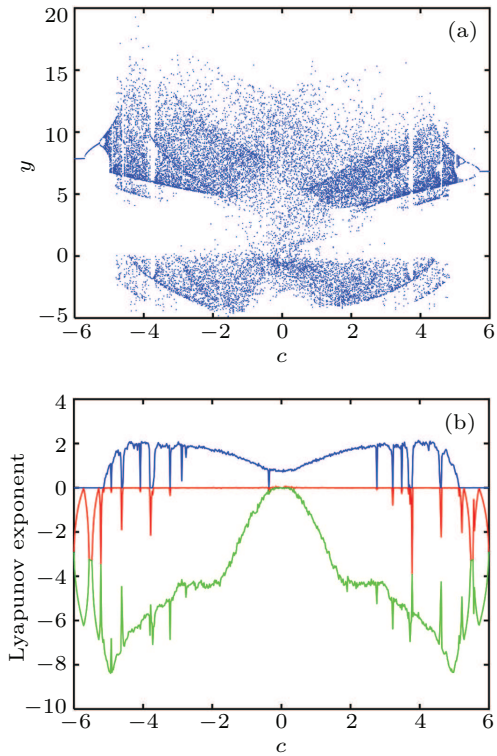


Fig. 3. Dynamical behaviors versus c: (a) bifurcation diagram, (b) LEs.

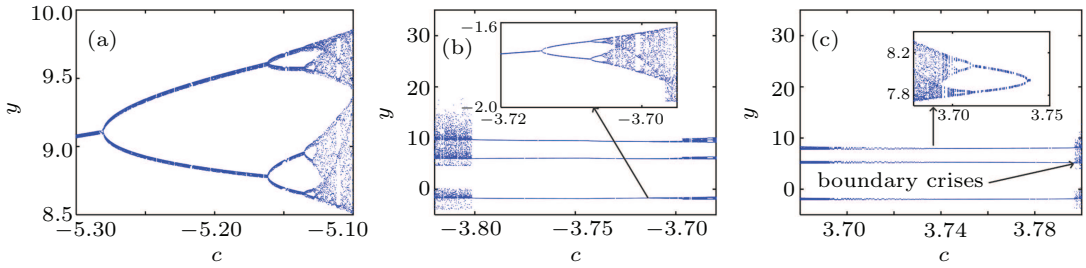


Fig. 4. Partial enlarged view of bifurcation: (a) and (b) partial enlarged view of period-doubling bifurcation, (c) partial enlarged view of reverse period-doubling bifurcation.

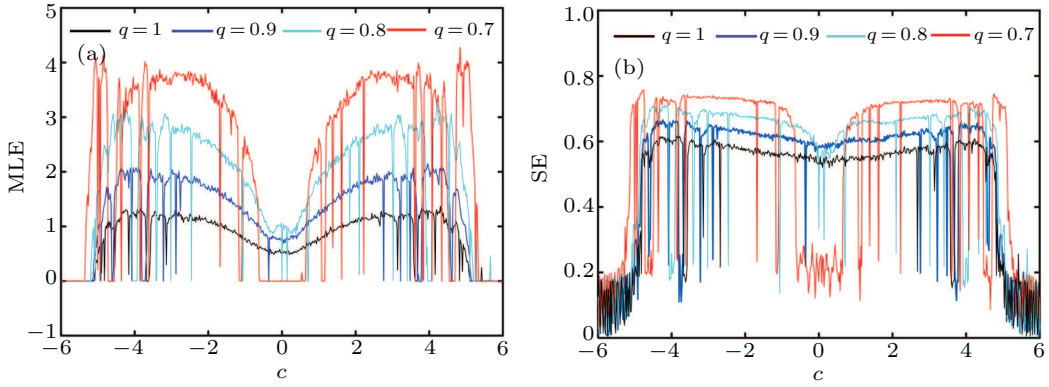


Fig. 5. The system performance versus c: (a) the MLE, (b) the SE complexity.

The changes of other bifurcation parameters and the corresponding first three LEs are shown in Fig. 6.

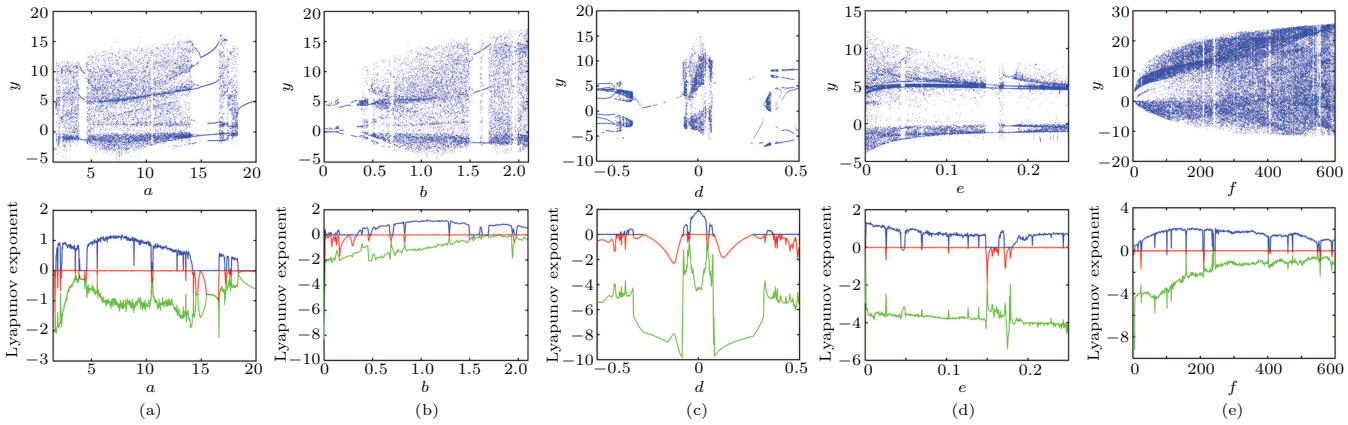


Fig. 6. The impact of parameters on system status with (a) parameter a, (b) parameter b, (c) parameter d, (d) parameter e, (e) parameter f.

3.2. Coexistence of attractors

Under three different initial conditions, the chaotic attractors coexist with two different sinks when $a = 10$, $b = 0.9$, $c = 0.8$, $d = -0.01$, $e = 0.088$, $f = 29$, $q = 0.9$, as shown in Fig. 7. In Fig. 7, the trajectories, with initial values of

$$x_0 = [3.26, -3.58, 3.6, -4.8, 36.2],$$
$$x_1 = [3.26, -3.58, 3.6, -4.8, 6.19],$$
$$x_2 = [3.26, -3.58, 3.6, -4.8, 36.18],$$

are represent by red, blue and green, respectively. It can be seen from the time domain diagram that both red and blue trajectories degenerate from the chaotic state to a sink, but the degeneration time and the final state position are different. However, the green trajectory always maintains the chaotic state. In addition, the MLE$x_2 > 0$ all the times, but the MLE$x_0 < 0$ after $t = 8675$ s and the MLE$x_1 < 0$ after $t = 3050$ s. The above discussion shows that small differences in initial values will lead to different final states of the system.

Figure 8 shows that the system has two coexisting weak chaotic attractors. Under the conditions $a = 8$, $b = 1$, $c = -1.68$, $d = -0.01$, $e = -0.005$, $f = 38$, $q = 0.7$, red is for the initial value $x_0 = [10, 0, 3, 1, -2]$, and blue is for the initial value $x_1 = [3.26, -3.58, 3.6, -4.8, 36.16]$. From the time-domain waveform and the evolution of LE over time, it can be seen that both the relatively weak chaotic attractors are transferred from the same strong chaotic attractor. However, the conversion times are different.

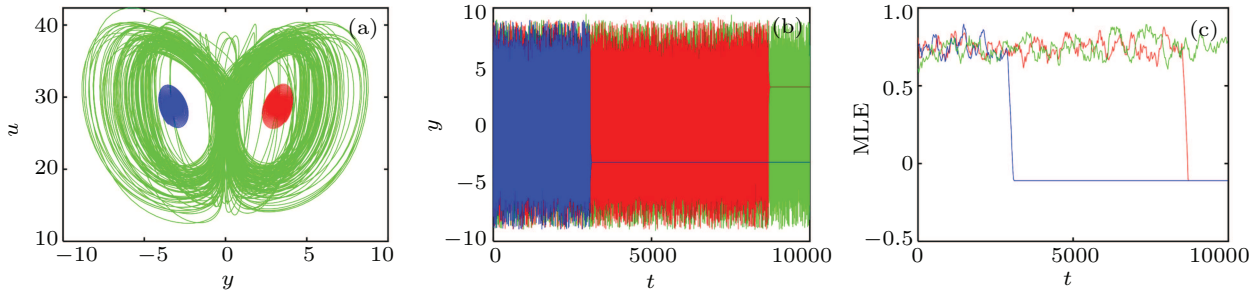


Fig. 7. Chaotic attractors coexisting with two sinks: (a) phase diagram, (b) the y waveform with different initial values, (c) the MLE changing with time under different initial values.

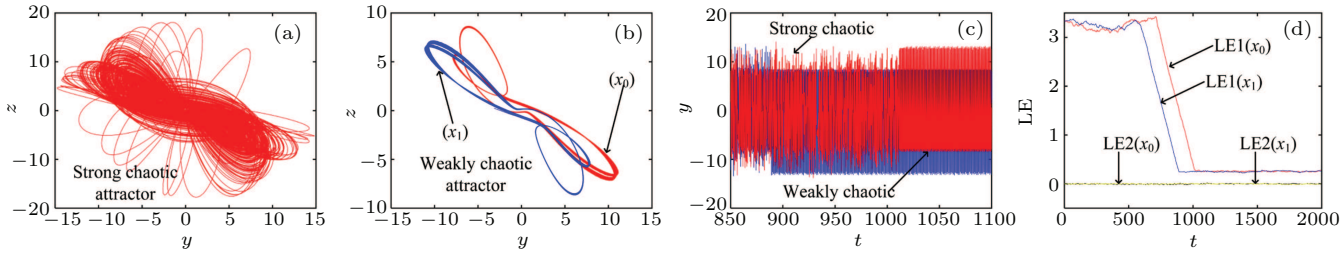


Fig. 8. Coexistence of two chaotic attractors: (a) strong chaotic state, (b) two different weakly chaotic state, (c) the y waveform with different initial values, (d) the first two LEs changing with time under different initial values.

The other types of coexisting attractors are shown in Fig. 9, and its corresponding parameters and the initial conditions are listed in Table 1.

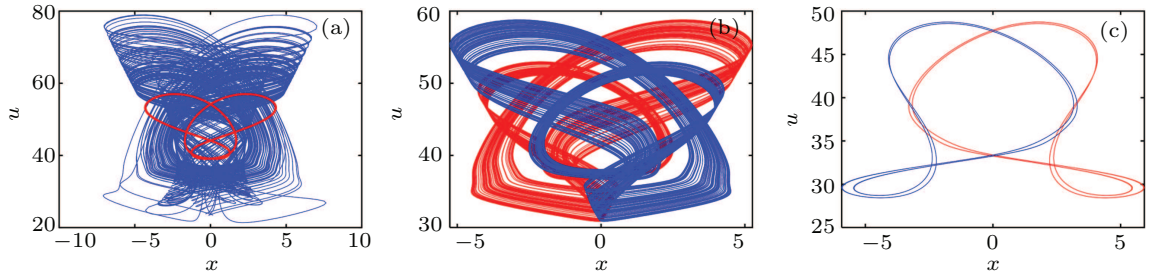


Fig. 9. Other types of coexisting attractors. (a) period-chaotic; (b) chaotic-chaotic; (c) period-period.

Table 1. The parameters, initial values, colors and coexisting type corresponding to Fig. 9.

Parameters	Initial conditions	Colors	Coexisting types
$a=8, b=1, c=-3.8, d=-0.3275, e=0.003, f=38, q=0.9;$	$x_0=[6,8,-8,5,40]$ $x_1=[3,4,-4,-5,38]$	red blue	period-chaotic
$a=8, b=1, c=-3, d=-0.3275, e=-0.005, f=38, q=0.9;$	$x_0=[6,8,-8,5,40]$ $x_1=[3,4,-4,-5,38]$	red blue	chaotic-chaotic
$a=8, b=1, c=-2.1, d=-0.3275, e=-0.005, f=38, q=0.9;$	$x_0=[6,8,-8,5,40]$ $x_1=[1,1,1,1,1]$	red blue	period-period

3.3. State transition and intermittent oscillation (breather)

When $a=8$, $b=1$, $c=-0.36$, $d=-0.01$, $e=-0.003$, $f=38$, $q=0.9$, the state of the system will shift with time, as shown in Fig. 10. Under these sets of parameters, the final periodic attractor is degenerated from the chaotic attractor, but the degradation time is 800 s for the initial value $x_0=[3.26,-3.58,3.6,-4.8,36.19]$, and 5100 s for the initial value $x_1=[1,1,1,1,1]$. Correspondingly, we have the MLEx_0, $x_1=0$ after 800 s and 5100 s, respectively.

When $a=8$, $b=1$, $c=3.797$, $d=-0.01$, $e=-0.005$, $f=38$, $q=0.9$, the time-domain waveform, LEs, and attractor that change with time are shown in Fig. 11. One can see from the time-domain waveform that the periodic oscillation of system state variables will be interrupted by random finite burst oscillations, and when the burst oscillation ends, the periodic oscillation will restart again. The trend of LEs changing with time can also prove that the system alternates between short-term chaos and periodic oscillation.

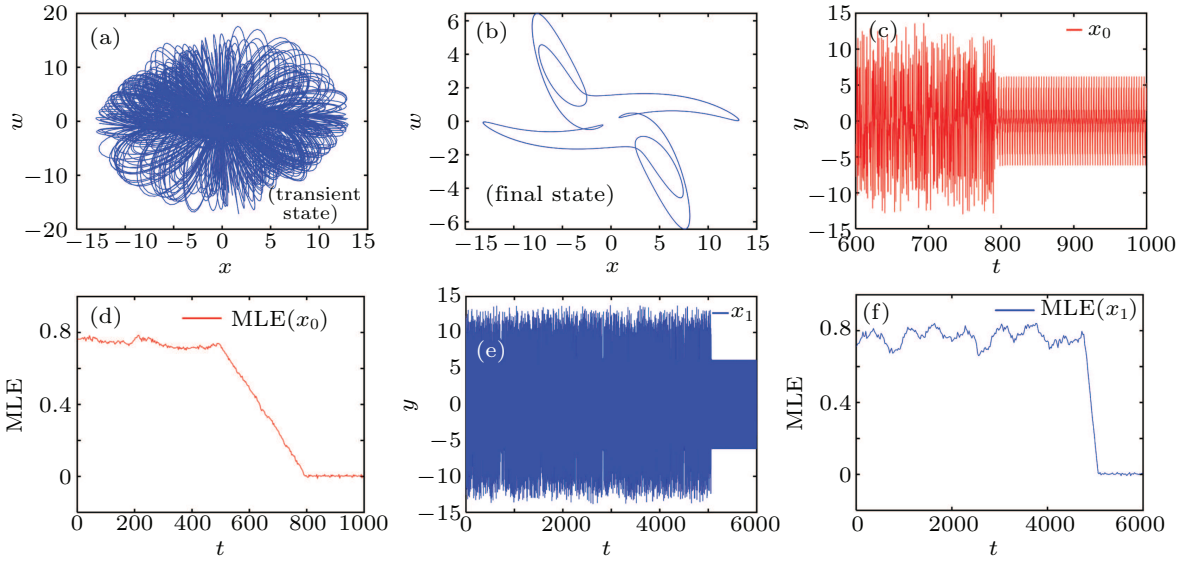


Fig. 10. Chaotic states degenerates to periodic state: (a) transient state, (b) final state, (c) the waveform of the y with x_0, (d) the MLE with x_0, (e) the waveform of the y with x_1, (f) the MLE with x_1.

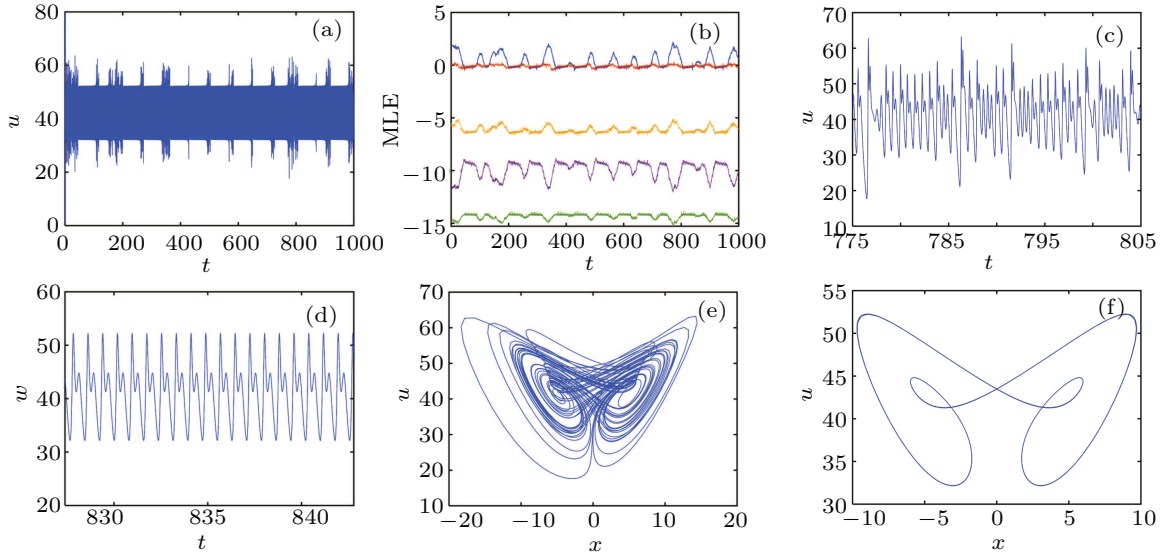


Fig. 11. Intermittent oscillation between the burst and periodic: (a) time-domain waveform, (b) the LEs changing with time, (c) the burst oscillation, (d) the periodic oscillation, (e) the burst oscillation attractor, (f) the periodic oscillation attractor.

3.4. Attraction basin and complexity analyzes

Using the attraction basin can easily find the parameters space of the system in a chaotic state, which is very effective in secure communication based on chaotic systems. Figure 12 detects the state distribution of the laser system on different parameter planes. In the figure, black represents the divergent state, red means stable point, yellow indicates periodic and blue means chaos. This means that the parameters corresponding to the blue area should be selected in chaotic cryptography.

In order to further find out the chaotic regions with high complexity, the spectral entropy complexity algorithm which can reflect the energy distribution of any signal in the frequency domain is considered here to measure the structural complexity of the FOCS, as shown in Fig. 13. The more balanced the energy distribution, the higher the complexity of the sequence structure, so the larger the SE value. The color levels are mapped to the level of system complexity. The initial value is setting as $x_0 = [1, 1, 1, 1, 1]$ and the parameters' conditions, maximum SE values and the corresponding coordinates are given in Table 2. One can see from a longitudinal point of view of Fig. 13(a) that, as q decreases, the complexity of the system becomes larger. However, when q is less than a certain value, the complexity of the system becomes smaller, and the system even diverges (white area). The maximum SE under this condition is 0.7703 with $a = 8.4$, $q = 0.65$. A larger SE value indicates that the fractional-order system can generate chaotic sequences with higher complexity.

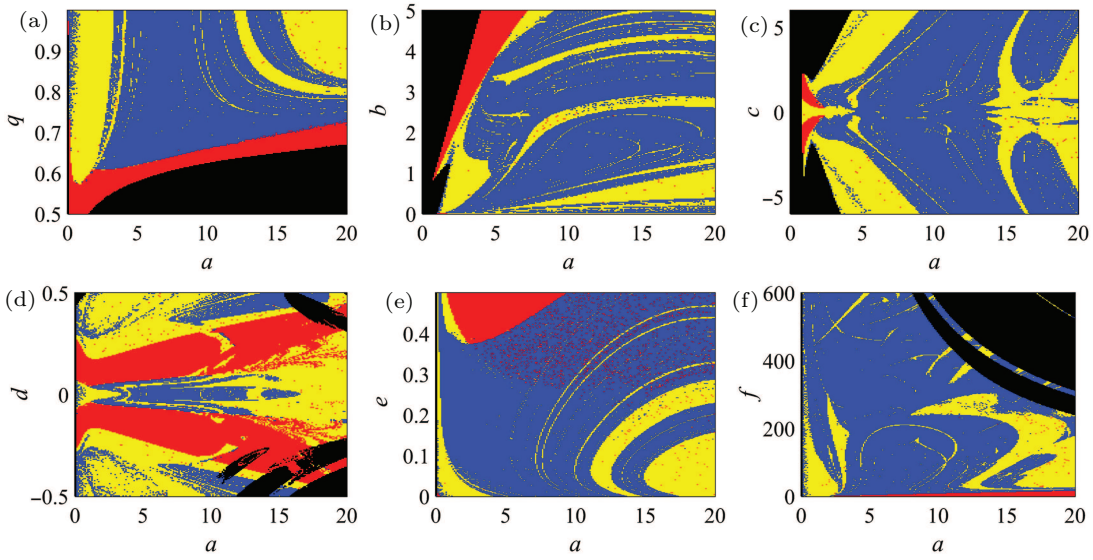


Fig. 12. The attraction basin with different parameters' planes: (a) a–q plane, (b) a–b plane, (c) a–c plane, (d) a–d plane, (e) a–e plane, (f) a–f plane.

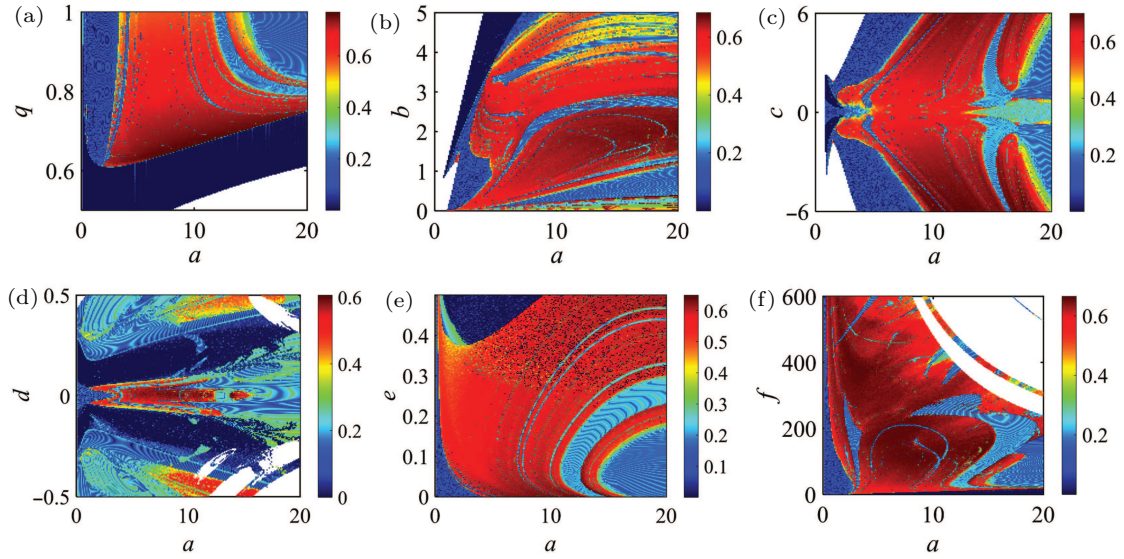


Fig. 13. SE complexity diagram of different parameters planes: (a) a–q plane, (b) a–b plane, (c) a–c plane, (d) a–d plane, (e) a–e plane, (f) a–f plane.

Table 2. Parameters of the SE complexity diagram (Fig. 13).

Parameters	Maximum SE	Corresponding coordinates
$b=1, c=2.1, d=0.01, e=0.01, f=38$	0.7703	$a=8.4, q=0.65$
$q=0.9, c=2.1, d=-0.01, e=-0.005, f=38$	0.6843	$a=19.3, b=0.375$
$q=0.9, b=1, d=-0.01, e=-0.005, f=38$	0.7	$a=10, c=-6$
$q=0.9, b=1, c=2.1, e=0.01, f=38$	0.648	$a=13.8, d=0$
$q=0.9, b=1, c=2.1, d=-0.01, f=38$	0.6492	$a=14.5, e=0.0025$
$q=0.9, b=1, c=2.1, d=0.01, e=0.02$	0.6655	$a=2.7, f=388$

4. The circuit realization of the FOLCS

Here, TMS320F28335 is used as the core processor to realize the 5-D FOLCS. The experimental system can be seen in Fig. 14.

Set the same parameters and initial value as in Fig. 1, and the DSP output sequence randomly intercepted on the oscilloscope is shown in Fig. 15.

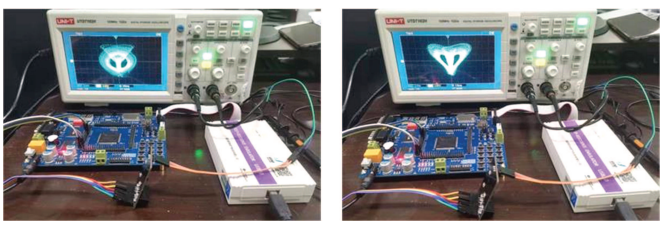


Fig. 14. The circuit test bench.

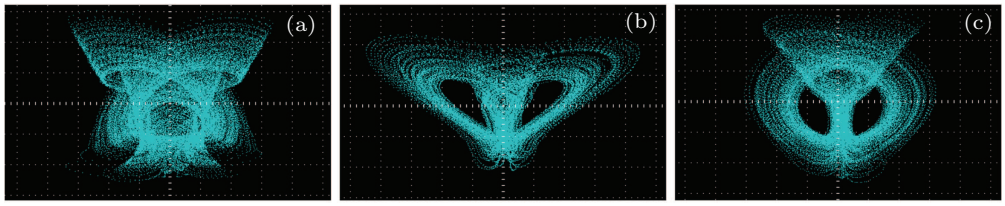


Fig. 15. The output sequences by DSP: (a) x–u sequence, (b) z–u sequence, (c) w–u sequence.

Compared Fig. 15 with Fig. 1, it can be seen that the DSP simulation results match well with the computer simulations. This indicates that the chaotic oscillation of the system can be realized on the DSP platform, which provides a guarantee for the application of the FOLCS.

5. PRNG based on the FOLCS

Pseudo-random numbers based on chaotic sequences play a vital role in image encryption, information hiding, digital authentication and other cryptographic fields. The seed of the PRNG can be the initial value and bifurcation parameters of the chaotic system. The output chaotic sequence x_i can be represented by a certain number of binary numbers, but there may be correlation between these numbers. Therefore, some of them can be selected to generated random sequence to reduce the correlation. Combining the parameters range given by the attractor basin and SE complexity chaotic diagram analyzed in Subsection 3.4, the chaotic region with high complexity should be selected as the seed of the PRNG. It is important to note that the divergence state of the black region, the stable point of the red area and the period state of the yellow area cannot be used as the seed of the PRNG. Algorithm 1 is the generation algorithm of this chaos-based pseudo-random sequence generator.

Algorithm 1. The the PRNG based on the FOLCS

Input: the parameters of the system.(2)
  For $i = 1$ to 5 do
    Get data Pi: intercept a section of the chaotic sequence x_i;
    Transform Pi to 32-bit binary;
    Extract the last 8 bits of the 32-bit binary;
  end for
Output: Five the PRNG based on x_i.

Table 3. The NIST test results.

Each sequence to be tested consists of 1000000 bits							
	NIST-800-22 tests	p-value(x)	p-value(y)	p-value(z)	p-value(w)	p-value(u)	Result
1	Block frequency ($m = 128$)	0.236810	0.834308	0.798139	0.419021	0.302137	Random
2	Frequency	0.946308	0.249284	0.122325	0.366918	0.687913	Random
3	FFT	0.699313	0.851383	0.739918	0.474986	0.091912	Random
4	Approximate entropy ($m = 10$)	0.319084	0.678686	0.816537	0.071177	0.313514	Random
5	Cumulative sums (Forward)	0.224821	0.108791	0.897763	0.181557	0.858961	Random
6	Serial-1 ($m = 16$)	0.224821	0.657933	0.494392	0.978072	0.789112	Random
7	Serial-2 ($m = 16$)	0.224821	0.851383	0.319084	0.834308	0.319762	Random
8	Runs	0.911413	0.419021	0.319084	0.851383	0.781921	Random
9	Longest run of ones	0.262249	0.145326	0.145326	0.798139	0.811792	Random
10	Overlapping template ($m = 9$)	0.181557	0.474986	0.419021	0.657933	0.401227	Random
11	Non-overlapping template ($m = 9$)	0.537714	0.489086	0.446348	0.475856	0.493137	Random
12	Linear complexity	0.350485	0.202268	0.554420	0.883171	0.971732	Random
13	Binary matrix rank	0.699313	0.026948	0.678686	0.419021	0.851437	Random
14	Universal statistical	0.262249	0.334538	0.739918	0.071177	0.383849	Random
15	Random excursions	0.521857	0.251909	0.617851	0.466935	0.462175	Random
16	Random Excursions Variant	0.416123	0.219526	0.444704	0.474079	0.421746	Random

There are many existing detection methods for random sequences, among which NIST test is the most widely used statistical detection method. The NIST-800-22 kit will evaluate the sequence from 16 different aspects and obtain a p value. It is generally believed that when the obtained p value is greater than 0.01, it is a random sequence with 99% confidence. Set the initial value $x_0 = [-3, 1, 5, 10, -7]$, parameters $(a,\ b,\ c,\ d,\ e,\ f,\ q) = (8, 1, -3.8, -0.3275, 0.003, 38, 0.9)$ are selected as the seed of the PRNG. Five PRNGs will be obtained according Algorithm 1, and each the PRNG contains 1000000 binary bits. The test results of NIST-800-22 are listed in Table 3.

6. Conclusion

By introducing the Caputo differential operator, this paper constructs a new 5-D FOLCS. The dynamical characteris-

tics of this system are analyzed by numerical solution. Compared to the corresponding integer-order system, the dynamical characteristics of the system in the fractional-order form are more complex, which is reflected in the fact that the maximum LE value of the system decreases with the increase of the order. The simulation results show that when the order $q = 0.9$, as the parameter c changes, the system not only has a larger LE value and SE complexity, but also has a larger parameter space making the system in a chaotic state. In addition, the laser system exhibits rich multi-stable behaviors, including the coexistence of chaotic attractors and two sinks, the coexistence of two symmetric chaotic attractors, and the coexistence of chaotic attractors and limit cycles. Meanwhile, there are two types of oscillation transitions in this system. One is that chaotic oscillations degenerate into periodic oscillations. The other is the endless alternate appearance of chaotic oscillation and periodic oscillation. The parameters corresponding to the high-complexity sequence that the system can generate are found through the SE complexity diagram. For example, when fixed $b = 1$, $c = 2.1$, $d = 0.01$, $e = 0.01$, $f = 38$, the maximum SE = 0.7703 when $a = 8.4$, $q = 0.65$. In addition, the simulation results of the digital circuit proposed in this article are consistent with the computer numerical simulation results, that is, the chaotic oscillation of the system is verified on the circuit. Finally, the PRNG based on the FOLCS has passed the NIST-800-22 test. In short, the theoretical and numerical simulation have proved that the FOLCS has rich chaotic characteristics. In the future, we will explore applications of this system in the field of image encryption.

References

[1] Zhang L M, Sun L J, Liu W J and He S B 2017 *Chin. Phys. B* **26** 100504
[2] Chai X L, Wu H Y, Gan Z H, Han D J and Chen C R 2020 *Inf. Sci.* **556** 305
[3] Hua Z Y, Zhu Z H, Yi S, Zhang Z and Huang H J 2020 *Inf. Sci.* **546** 1063
[4] Lan R S, He J W, Wang S H, Gu T L and Luo X N 2018 *Signal Processing***147** 133
[5] Wang M X, Wang X Y, Wang C P, Xia Z Q, Zhao H Y, Gao S, Zhou S and Yao N M 2020 *Chaos Soliton Fract.* **139** 110028
[6] Yang F F, Mou J, Liu J, Ma C G and Yan H Z 2020 *Signal Processing* **169** 107373
[7] Xu C, Sun J R and Wang C H 2020 *Int. J. Bifurcat. Chaos* **30** 2050060
[8] Peng Y X, Sun K H and He S B 2020 *Chin. Phys. B* **29** 30502
[9] Liu J, Tong X J, Liu Y, Zhang M and Ma J 2018 *Nonlin. Dyn.* **93** 1149
[10] Li H Z, Hua Z Y, Bao H, Zhu L, Chen M and Bao B C 2020 *IEEE Trans. Industrial Electron.* **68** 9931
[11] Yang F F, Mou J, Ma C G and Cao Y H 2020 *Opt. Laser Eng.* **129** 106031
[12] Xu Q Y, Sun K H, Cao C and Zhu C X 2020 *Opt. Laser Eng.* **121** 203
[13] Han M, Li W J, Feng S B, Qiu T, Chen C L P 2020 *IEEE Trans. Neual Networks Learning Sys.* **32** 2320
[14] Zhang A and Zheng X 2020 *Cognitive Neurodynamics* **14** 849
[15] Zheng J and Hu H P 2020 *Chin. Phys. B* **29** 090502
[16] Abdulaziz, O, A, Alamodi, Sun K H, Chen C and Peng C 2019 *Chin. Phys. B* **29** 20503
[17] Singh J P, Pham V T, Hayat T, Jafari S, Alsaadi F E and Roy B K 2018 *Chin. Phys. B* **27** 100501
[18] Wang G Y, Jin P P, Wang X W, Shen Y R, Yuan F and Wang X Y 2016 *Chin. Phys. B* **25** 090502
[19] Hu X Y, Liu C X and Liu L 2017 *Chin. Phys. B* **26** 110502
[20] Cheng M F, Luo C K, Jiang X X, Deng L, Zhang M M, Ke C J, Fu S N, Tang M, Shum P and Liu D M 2018 *J. Lightwave Technol.* **39** 18072943
[21] Wang L S, Mao X X, Wang A B, Wang Y C, Gao Z S, Li S S, Yan L S 2020 *Opt. Lett.* **45** 4762
[22] Yang Z, Yi L L, Ke J X, Zhu G Q B, Yang Y P and Hu W S 2020 *J. Lightwave Technol.* **38** 4648
[23] Yan S L 2018 *Appl. Mech. Mater.* **876** 147
[24] Li N Q, Nguimdo R M, Locquet A and Citrin D S 2018 *Nonlin. Dyn.* **92** 315
[25] Jiang X, Xiao Y, Xie Y Y, Liu B C, Ye Y C, Song T T, Chai J X and Liu Y 2021 *Opt. Commun.* **484** 126683
[26] Shahzadi R, Anwar S M, Qamar F, Ali M, J. J. P. C. Rodrigues and Alnowami M 2019 *IEEE Access* **7** 57769
[27] Wang D M, Wang L S, Guo Y Y, Wang Y C and Wang A B 2019 *Opt. Express* **27** 3065
[28] Santo B, Papri S and Chowdhury A R 2001 *Phys. Lett. A* **291** 103
[29] Al-Kouz W, Al-Muhtady A, Owhaib W, Al-Dahidi S, Hader M and Abu-Alghanam R 2019 *Entropy* **21** 103
[30] Ran C, Tang X, Wu Z M and Xia G Q 2018 *Laser Phys.* **28** 126202
[31] Kar R 2018 *CSI Trans. ICT* **7** 175
[32] He S, Sun K H, Wang R X. 2018 *Eur. Phys. J. Spec. Top.* **227** 943
[33] Khajehnasiri A A, Afshar Kermani M and Ezzati R 2020 *Int. J. Math. Operat. Res.* **17** 1
[34] Pu Y F, Zhang N and Wang H 2020 *IEEE Intellig. Sys.* **35** 19610601
[35] Pu Y F, Yu B and Yuan X 2020 *IEEE Design & Test* **38** 104
[36] He S B 2020 *Front. Appl. Math. Statis.* **6**
[37] Abdeljawad T 2015 *J. Comput. Appl. Math.* **297** 57
[38] Zhou H W, Yang S and Zhang S Q 2015 *Physica A* **491** 1001
[39] Silva-Juáreza A, Tlelo-Cuautlea E, la Fragab L G and Li R 2020 *J. Adv. Res.* **25** 77
[40] He S B, Sun K H and Wu X M 2020 *Phys. Scr.* **95** 035220
[41] Peng Y X, Sun K H, He S B 2020 *Eur. Phys. J. Plus* **135** 331
[42] He S B, Santo B and Sun K H 2019 *Eur. Phys. J. Spec. Top.* **228** 331
[43] Ye G D, Jiao K X, Wu H S, Pan C and Huang X L 2020 *Int. J. Bifurcat. Chaos* **30** 2050233
[44] Zhou C Y, Li Z J, Zeng Y C and Zhang S 2020 *Int. J. Bifurcat. Chaos* **29** 1950004
[45] Ding D W, Shan X Y, Jun L, Hu Y B, Yang Z L and Ding L H 2020 *Mod. Phys. Lett. B* **34** 2050191
[46] He S B, Sun K H, Wang H H, Mei X Y and Sun Y F 2017 *Nonlin. Dyn.* **92** 85
[47] Yu Y J, Shi M, Kang H Y, Chen M and Bao B C 2020 *Nonlin. Dyn.* **100** 891
[48] Wang M J, Liao X H, Deng Y, Li Z J, Zeng Y C and Ma M L 2019 *J. Comput. Nonlin. Dyn.* **14** 071002
[49] He S B, Santo B and Sun K H 2018 *Chaos Soliton Fract.* **115** 14
[50] Ma C G, Mou J, Liu J, Yang F F and Zhao X 2020 *Eur. Phys. J. Plus* **135** 95
[51] Wang M J, Liao X H, Deng Y, Li Z J and Zeng Y C 2020 *Chaos Soliton Fract.* **130** 109406